Electronic Supplementary Information (ESI) for

Li-ion transport at interface between graphite anode and Li_2CO_3 solid electrolyte interphase: Ab-initio molecular dynamics study

Takeshi Baba[†], Keitaro Sodeyama[‡,§], Yoshiumi Kawamura[†,] , Yoshitaka Tateyama[‡,§,⊥,*]*

† Frontier Research Center, Toyota Motor Corporation, 1200, Mishuku, Susono, Shizuoka, 410-1193, Japan

‡ Center for Materials Research by Information Integration (cMI^2), Research and Services Division of Materials Data and Integrated System (MaDIS), National Institute for Materials Science (NIMS), 1-1 Namiki, Ibaraki 305-0044, Japan

§ Elements Strategy Initiative for Catalysts and Batteries(ESICB), Kyoto University, Goryo-Ohara, Nishikyo-ku, Kyoto 615-8245, Japan

⊥ Center for Green Research on Energy and Environmental Materials (GREEN) and International Center for Materials Nanoarchitectonics (MANA), NIMS, 1-1 Namiki, Tsukuba, Ibaraki 305-0044, Japan

S1. Model of Li-intercalated graphite

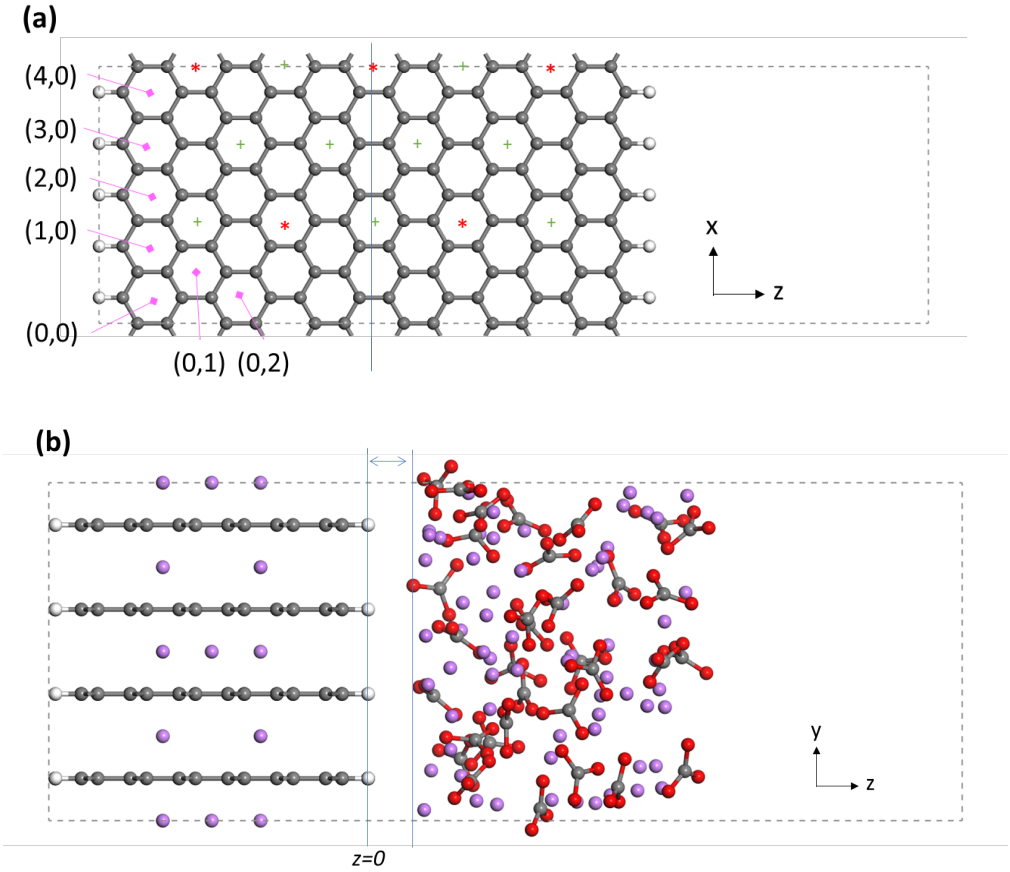

Fig. S1 (a) In-plane display of Li-intercalated graphite model ($C_{480}H_{20}$). Gray and white balls show C, H atoms, and the asterisk (red) and plus (green) marks denote Li ions of intercalated-layer α_1 and α_2, respectively. The relative intercalated sites are also shown in the parentheses. C_{240} model were terminated by the border shown by the blue line. (b) An example structure combining $Li_{10}C_{240}H_{20}$ graphite model with 33 Li_2CO_3 SEI model. Gray, white and purple ball (in colors) show C, H and Li ions, respectively. The two blue lines indicate interlayer distance. The left line also plays a role of the z-coordinate origin, which is introduced to discuss the interface properties (e.g. free energy profile of the Li^+ insertion process).

First, the graphite models with AA-stacking and four layers were prepared as follows. For the graphite sheet, a lattice with P6/mmm group was used. The parameters were set to a(=b)=2.471 and c=3.700 Å, which correspond to the experimental values of LiC_6[S1], including two C atoms with the fractional coordinates; (2/3, 1/3, 1/2) and (1/3, 2/3, 1/2). The lattice vectors were redefined as [a:5 5 0, b:-3 3 0, c:0 0 4] and [a:5 5 0, b:-6 6 0, c:0 0 4], which represent C_{240} (5x5 rings) and C_{480} (11x5) models respectively. Then, the cell vector was reoriented (a,b,c) to (x,z,y), where the z length was elongated to introduce vacuum region and made the zig-zag edge. H, OH, or COOH group was added to the edge carbon atoms to terminate appropriately as described in the main article.

Next, intercalated Li layers were arranged. Denoting the layer as α, we consider -A-α_1-A-α_2-A-α_1-A-α_2-(A-…) stacking model. Now, the left-bottom intercalation cite is defined as the origin (0,0), and the relative cites (x,y) are defined as shown in Fig.S1a. The Li-ions locate at (4,1)*, (1,3)*, (4,5), (1,7), (4,9) in the α_1, and (1,1)*, (3,2)*, (4,3)*, (3,4), (1,5), (3,6), (4,7),

(3,8), (1,9) in the α_2, where the asterisk suggests the case of C_{240} model.

Amorphous SEI part was built by the Amorphous Cell Construction task in the Materials Studio program[S2]. The construction lattice type was set to "Orthorhombic" with a=12.36 and b=14.80 Å (which is the same as the graphite models), the density was set to the experimental value (2.11 g/cm^3)[S3], and the composition is the same number of Li^+ ions and CO_3^{2-} molecules (c length was automatically defined using the density and composition). Note that the construction of pure amorphous structure uses almost the same procedure, although the lattice type was set to "cubic". The constructed structure put into the graphite model near edge. The z-distance of the graphite edge (top of terminated atom) and SEI was initially set to approximately 2 Å (See Fig. S1b). Since the SEI structure was generated without the graphite edge effect and the interface matching was quite rough, the careful MD equilibration is required. However, in our five-individual trials for each three-type terminated model, no unphysical behavior such as dissociation of graphite and SEI layer was observed.

S2. Calculated radial distribution functions (RDFs) of amorphous and crystalline Li_2CO_3

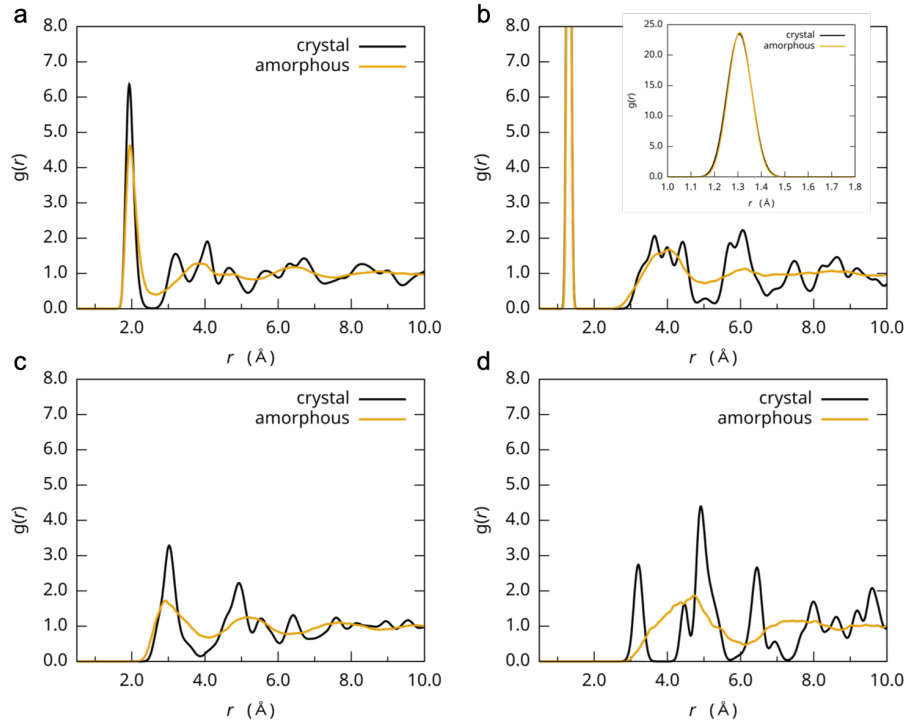

Fig. S2 Radial distribution function (RDFs), g(r), of (a) Li-O, (b) C-O, (c) Li-Li, and (d) C-C in the amorphous (yellow) and crystalline (black) Li_2CO_3 bulk systems. Inset figure in b is enlarged in the first peak.

Fig. S2 shows the calculated radial distribution functions (RDFs) of Li-O, C-O, Li-Li, and C-C in the amorphous and crystalline Li_2CO_3 bulk systems. Regarding the first sharp peak of Li-O, the peaks in the amorphous and crystalline systems are located at 1.96 and 1.93 Å, respectively. Those of C-O, which correspond to C-O bond distance of CO_3^{2-} moiety, are at both 1.31 Å and highly overlapped. Thus, no difference in CO_3^{2-} moiety exists between amorphous and crystalline environments. The values are in good agreement with the experimental ones of the crystalline Li_2CO_3 (1.958 Å of Li-O and 1.281 Å of C-O)[S3]. First sharp peaks of Li-Li in the amorphous and crystalline systems lie at 2.91 and 3.02 Å, respectively. The amorphous one is slightly shifted and broadened, and also the gap between the first and second peaks is unclear. This tendency was also found in the Li-O distribution. It is suggested that the interaction between Li^+ and CO_3^{2-} is in the same order for both amorphous and crystalline systems, though the amorphous phase has less symmetry restriction. Furthermore, the first peak of C-C in amorphous disappeared, indicating the distances and orientations of CO_3^{2-} moieties involve disorder. The mass densities are 1.88 and 2.04 g/cm^3 for the amorphous and crystalline models, respectively. The amorphous phase has slightly larger volume due to the disorder.

S3. Distribution of the Li-O coordination in amorphous and crystalline Li_2CO_3

Table S1 Distribution of the bond type of Li-ions for binding to O in the amorphous and crystalline Li_2CO_3. Averages over distinct three geometries are shown in percentage. Bond criterion of Li-O is 2.4 Å.

		amorphous				**crystalline**			
		number of binding molecules							
		2	3	4	5	2	3	4	5
number of bonds	3	1.6	20.8	--	--	--	2.1	--	--
	4	1.0	17.7	41.1	--	--	--	97.9	--
	5	--	6.3	9.9	1.0	--	--	--	--
	6	--	--	0.5	--	--	--	--	--

S4. Defect formation energies for amorphous and crystalline Li_2CO_3

Table S2 Li vacancy formation energies depending on the coordination situations of Li-ion for amorphous and crystalline Li_2CO_3. Since this evaluation was performed for one snapshot of Li_2CO_3, some figures (in italic) were based on one result (i.e. not averaged) and some binding patterns (labeled by asterisk mark) were missing.

		amorphous				**crystalline**			
		number of binding molecules							
		2	3	4	5	2	3	4	5
number of bonds	3	*-4.36*	-4.50	--	--	--	-4.91	--	--
	4	*-4.57*	-4.38	-4.62	--	--	--	-4.95	--
	5	--	-4.41	-4.68	*	--	--	--	--
	6	--	--	*	--	--	--	--	--

S5. Formation energies of amorphous and crystalline Li_2CO_3

For arguing the stability of amorphous and crystalline Li_2CO_3, the energy difference in the reaction $Li_2CO_3(s) \rightarrow Li_2O(s) + CO_2(g)$ was estimated. The calculated energy difference for the amorphous and crystalline Li_2CO_3 were -1.35 and -1.77 eV, respectively. While the experimental value based on free energy at 298 K[S4] was -2.32 eV and the other computational ones by accurate DFT study[S5] with (without) phonon effect and free energy of CO_2 was -2.33 (-2.11) eV, our results were relatively smaller in absolute value. Since present calculations did not involve free energy of CO_2, our results were adequate to describe the reaction energy. In comparison between amorphous and crystalline Li_2CO_3, the crystalline phase is more stable as expected. However, the amorphous was enough to be realized in reality.

S6. Computational details for the defect migration energies of crystalline Li_2CO_3

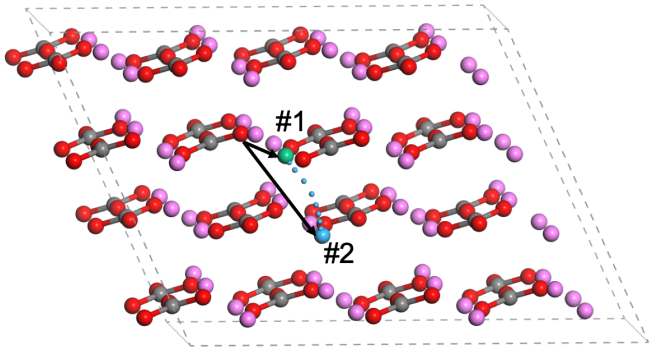

Fig. S3 Reaction coordinate of Li vacancy migration in the crystalline Li_2CO_3. The vacancy Li site of #1 and #2 were displayed by green and blue balls, respectively, which correspond to the coordinates of 0 and 4 for the diffusion in the previous work.[S6] Li (as well as vacancy) migrates between the two sites and the ideal path are denoted in small blue balls. Constraint coordinate was set to the distance between migrated Li and O that are nearest to the vacancy site #1, which is shown as a black arrow. Gray, red and purple ball (or line) show C, O, and Li atoms, respectively.

To confirm the migration energy of Li vacancy in the crystalline Li_2CO_3 by constrained DFT-MD technique using the CPMD code, we chose the most stable pathway reported by the previous work[S6]. Fig. S3 showed the migration pathway and the coordinate definition to constrained DFT-MD. In this study, constraint coordinate was defined as the distance between the migrated Li and O that are nearest to the vacancy site #1. In detail, Li at site #1 was removed and then Li at site #2 migrated to #1 with changing the coordinate constantly (by 0.25 Å) to obtain the set of potential of mean force. Opposite migration (#1 to #2) was also evaluated and averaged profile was used. For better understanding of migration profile, the constraint coordinate was projected to relative distance of migrated Li^+ from the vacancy site #1 (See Fig. 2c).

S7. Electronic states of amorphous and crystalline Li_2CO_3

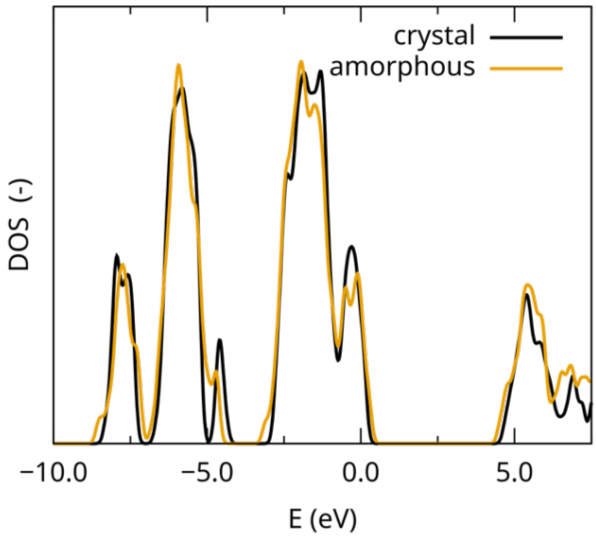

Fig. S4 Density of states (DOS) of amorphous (yellow) and crystalline (black) Li_2CO_3.

We also calculated the averaged electronic states (density of states (DOS)) to examine the electronic conductivity. Fig. S3 shows DOSs of the amorphous and crystalline Li_2CO_3. They are quite similar. In detail, the band gap of the amorphous (3.4 eV) is smaller than that of the crystalline phase (3.7 eV), because of the disorder. The variety of the geometrical structures in the amorphous causes the valence band peak broadening that makes the band gap of amorphous smaller.

S8. Computational details for Li migration of Li-intercalated Graphite

Li migration of internal and subsurface region using separated graphite model (see Fig. 1c) as well as Li transition from Li_2CO_3 part to interstitial Li_xC_6 using graphite-SEI interfacial model (Fig.1d and 4) were calculated by the constraint DFT-MD with Blue-moon ensemble method. In common with the Li vacancy migration in the crystal Li_2CO_3 as described in S6 of ESI, constrained coordinates were defined as the distance of migrated Li and a reference atom that is chose from intercalated Li atoms. In case of regional migration using graphite-separated model, the atom at two-site prolonged along intercalated position (2)→(0) (See Fig. 3) in the intercalated layer, which migrated Li was added, was set to the reference atom. The differential constrained coordinate to obtain the set of potential of mean force was set to 0.62 Å, which is quarter of the distance between intercalated position.

In case of insertion process using graphite-SEI interface model, the migrated Li was chose from the nearest Li to graphite-edge among SEI component and the reference atom was set to the intercalated Li in the layer which was defined by using side-plane (y-axis in Fig S1b) coordinate of the migrated Li. The differential coordinate was set to 0.5 Å.

S9. Another radial distribution function between graphite edge and SEI components

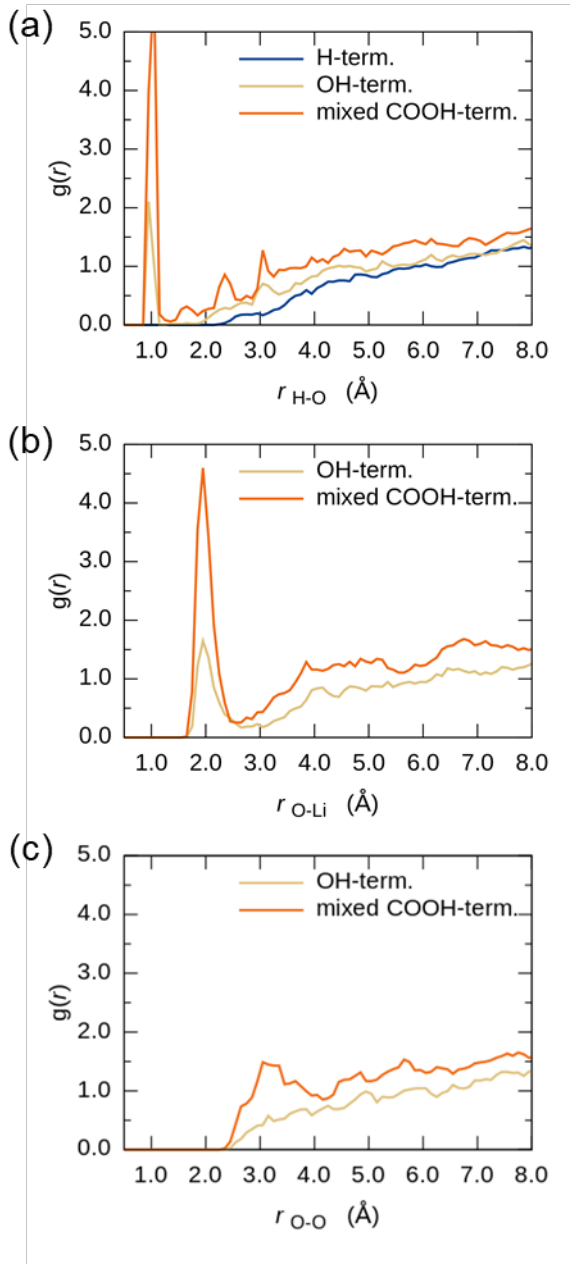

Fig. S5 Radial distribution functions of (a) H in the graphite termination and O in SEI, (b) O in the graphite termination and Li in SEI, and (c) O in the graphite and O in SEI for the interface models of H-, OH-, and mixed COOH-termination.

S10. Another sampling for Li^+ migration from Li_2CO_3 SEI to LiC_{24} graphite anode by the constrained DFT-MD technique

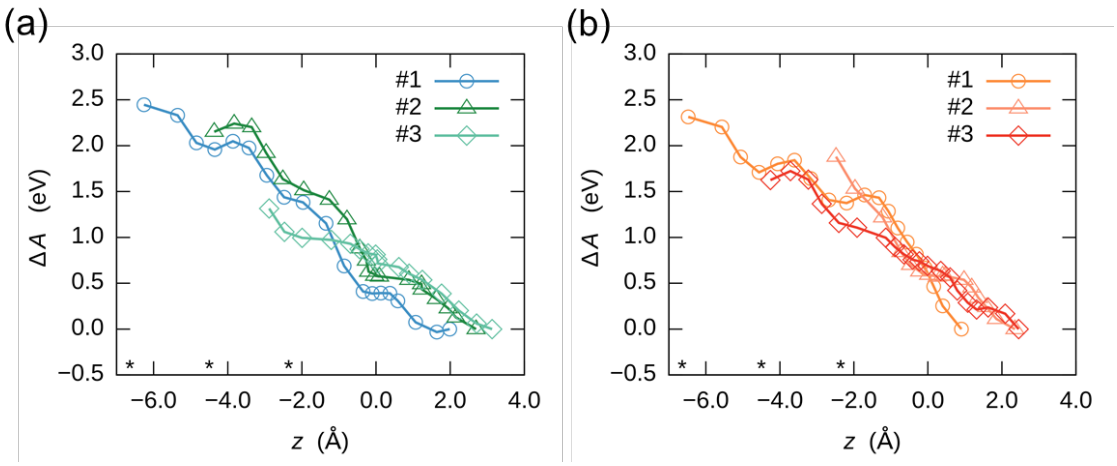

Fig. S6 Free energy profiles by constrained DFT-MD calclulations for (a) the H-termination and (b) the mixed COOH-termination model. Three distinct samplings were performed for each model. Asterisks at the horizontal axis indicate intercalation positions in graphite.

S11. Li^+ migration from Li_2CO_3 SEI to LiC_{24} graphite anode under three transferred Li conditions

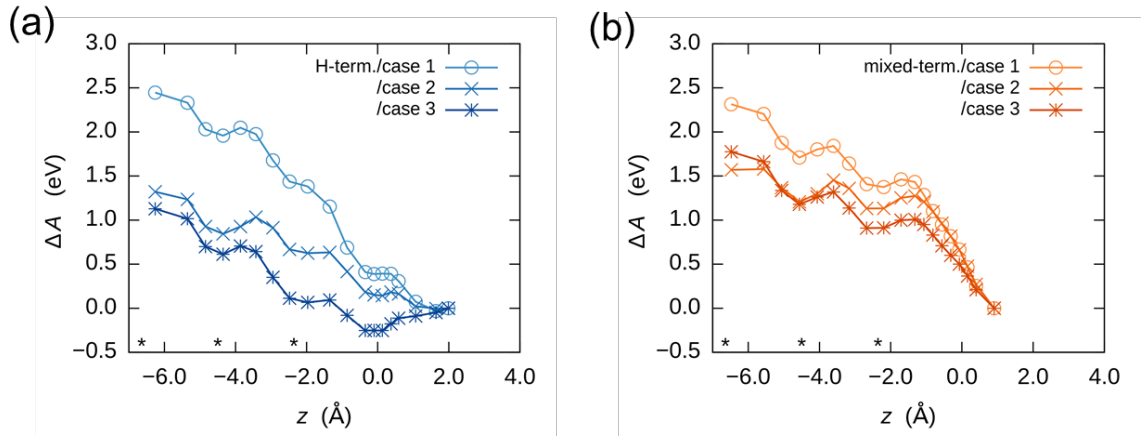

Fig. S7 Free energy profiles with transferred Li^+ conditions by constraint DFT-MD for (a) the H-termination and (b) the mixed COOH-termination model. Case means the target Li+ situation, which is explained in Fig. 6. Asterisks at the horizontal axis indicate intercalation positions in graphite.

S12. Structural change upon Li^+ intercalation from the Li_2CO_3 SEI to LiC_{24} graphite anode

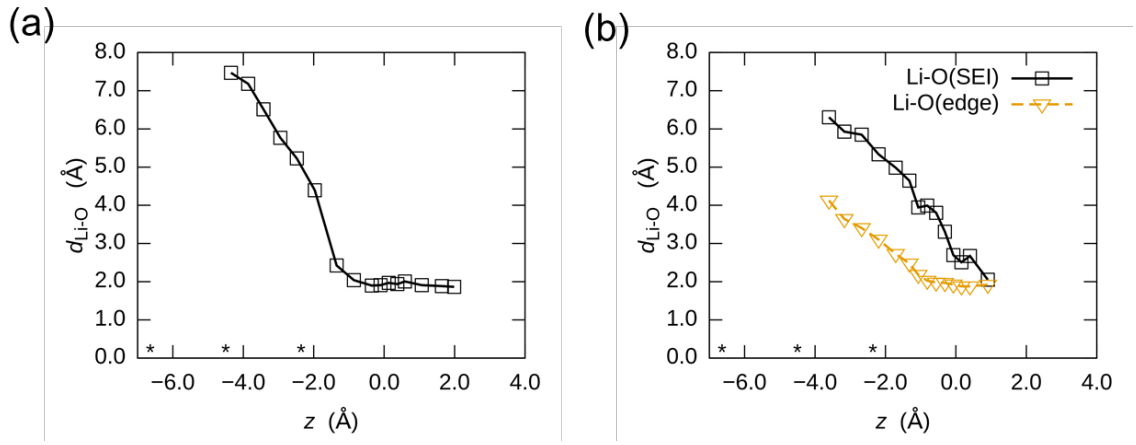

Fig. S8 Distance of the nearest neighbor O consisting of Li_2CO_3 SEI and the terminated edge of graphite from target Li-ion at coordinates in the constraint DFT-MD. (a) In the case 1 simulation of H-termination and (b) that of mixed COOH-termination. Asterisks at horizontal axis indicate intercalation positions in graphite.

We investigated the geometrical change upon Li^+ intercalation, with the average distances of target Li^+ and the neighbor Oxygen atoms in the case 1. In the H-termination, the distance between the target Li^+ and counterpart O in the CO_3^{2-} moiety does not change between z=2 and z=-1. This means that the CO_3^{2-} moiety is associated with Li^+ till the interface. The increase of distance for z<-2 indicates that the association is taken apart inside the graphite. For the mixed COOH termination, we draw the two distances to Oxygen in the CO_3^{2-} and Oxygen in the termination (COOH or OH). The results indicated that the O in the CO_3^{2-} does not show a plateau, while does the terminated O. This suggests that the target Li^+ easily dissociates with the CO_3^{2-} moiety before intercalation and the termination O follows the Li^+ intercalation for a while. The former implies that the bulky COOH group interferes with CO_3^{2-}. These results suggest that the co-intercalation of CO_3^{2-} moiety has large probability in the H-termination.

S13. Averaged atomic charge for elemental components in anode by the Bader charge analysis

Table S3 Averaged atomic charge for elemental components in anode by the Bader charge analysis. C in graphite were categorized by row into C1, C2, C3, C4, C5, and C6, which have the z coordinate ranges of (-12.47 and -11.76), (-10.33 and -9.62), (-8.19 and -7.48), (-6.05 and -5.34), (-3.91 and -3.20), and (-1.77 and -1.06), respectively. H in graphite are also categorized into two parts: external (z=-13.5) and interface (0). All values were averaged over distinct six geometries.

		H-termination		mixed COOH-termination	
		case 1	case 3	case 1	case 3
graphite	$H_{external}$	0.041	0.034	0.040	0.040
	C1	-0.012	-0.010	-0.012	-0.014
	C2	-0.045	-0.048	-0.046	-0.049
	C3	-0.073	-0.059	-0.063	-0.055
	C4	-0.064	-0.081	-0.072	-0.082
	C5	-0.053	-0.045	-0.045	-0.040
	C6	-0.016	-0.023	0.098	0.093
	$H_{interface}$	0.048	0.013	0.083	0.084
	Li	0.876	0.876	0.875	0.875
functional	C			1.420	1.342
	O			-1.172	-1.188
	H			0.644	0.641

In order to understand the underlying chemistry, we evaluated atomic population by the Bader charge analysis. Table S3 shows the averaged net charge over elements belong to anode. Note that the values of C in graphite were separated by z coordinate into six parts. While outermost C atoms (C6 in Table S3) in H-termination have negative charge slightly as ca. -0.02, that in mixed COOH-termination polarized moderately positive as ca. 0.09. The other parts were no significantly different between the terminations. Because in case of mixed COOH-termination migrated Li^+ was repulsive with positive outermost C atom, profiles showed monotonic increased around z=0, modest barrier at z=-1.3, and also relatively high at intercalated site 1 (z=-2.5) relative to the H-termination case. However, following migration (z=-2.5 to -4.6) has the advantage that it leaves positive C atoms, resulting in smaller barrier than the case of H-termination. Then, energy profiles at inner region of both terminations lead to nearly identical.

Table S3 also showed the charging effect (difference of case 3 from case 1). In case of H-termination, H atoms of interface edge ($H_{interface}$ in Table S3) were changed remarkably. Induced electron was delocalized at edge, which is corresponding to less slope of energy profile. Whereas, in case of mixed COOH-termination, H of interface edge have no change but

C in functional group was decreased remarkably. O in functional group was also changed modestly. It corresponds to C of carbonyl group had positive charge due to neighbor O with strong electron-withdrawing. When charging process, the delocalization of carbonyl C atoms were slightly relieved but remained largely positive, and that of other O and H in functional group showed no change. This is due to limited energy shift with relative to case of H-termination. Note that it is seem to the net charge of C3 and C4 were varied between case 1 and case 3 in both H and mixed terminations. Considering C3 and C4 as 6-membered ring, they do not change in the charging process because mean of those were kept ca. -0.07 for each case. These atoms were more negative than the other C atoms. This is due to the neighbor Li-ion. Averaged Li-ion charge is ca. 0.88 for each case, indicating that Li-ion in graphite is kept to be cation under Bader charge analysis.

S14. Gross population for anode and its component with regard to the position of migrated Li^+

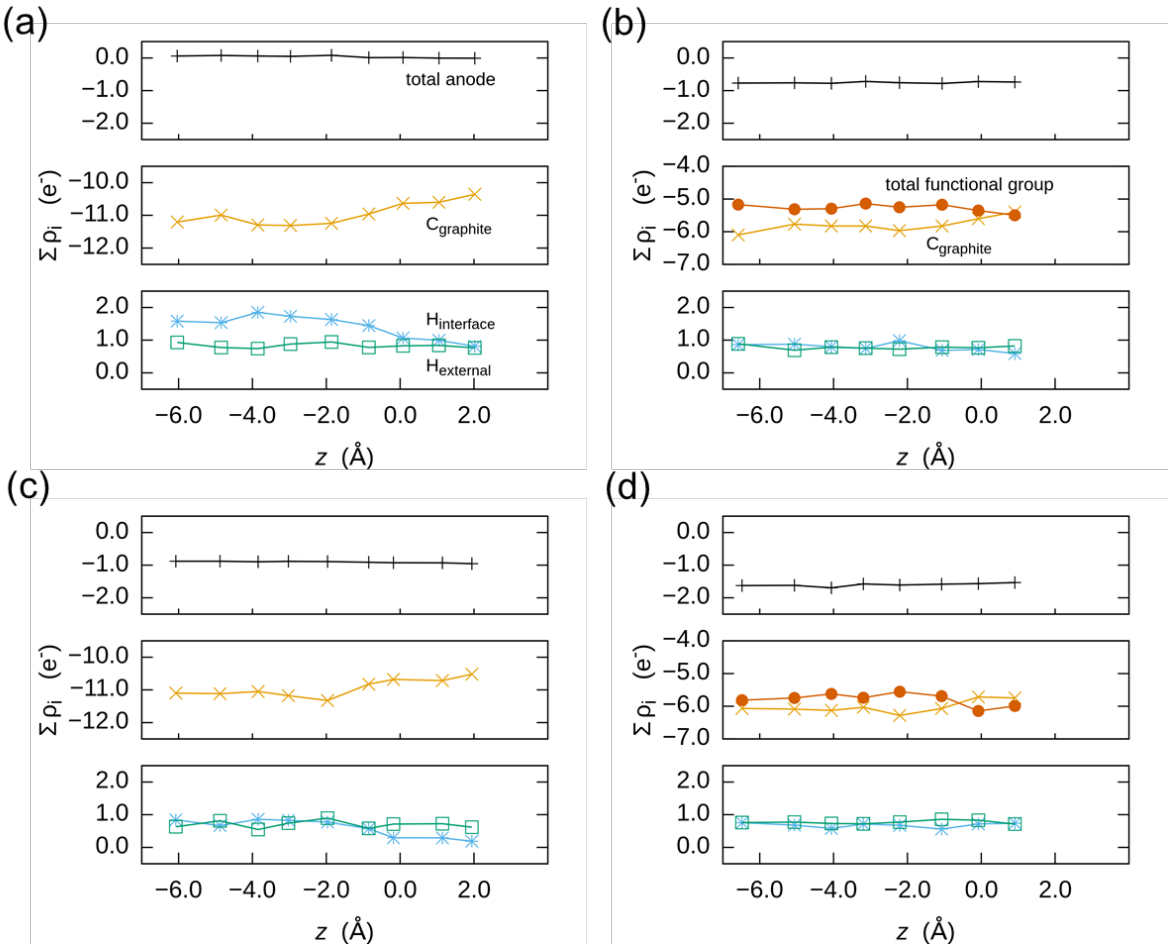

Fig. S9 Gross population for anode and its component with regard to the position of intercalated Li-ion: (a) case 1 and (c) case 3 for the H-termination and (b) case 1 and (d) case 3 for the mixed-COOH termination. Top figure is net population of total anode ($C_{240}Li_{10}H_{40}$/$C_{244}Li_{10}H_{40}O_{16}$ in the H- and mixed-COOH terminations, respectively), middle and bottom ones show the components such as C atoms consisting of graphite (C_{240}; plot with cross mark) and, interface (H_{20}; asterisk and light blue) and external (H_{20}/H_8; open square and green) of terminal H, and terminal COOH and OH groups ($C_4H_{12}O_{16}$; filled circle and brown). Note that the values of Li-ions intercalated in graphite were abbreviated because they have almost constant value (8.75 for Li_{10}) for all cases.

In order to investigate the charge variation with regard to the Li-ion intercalation process, gross population of total as well as major components of anode are shown in Fig. S8. Total charges of anode were almost constant during the intercalation for any case. The difference between case 1 and 3 was almost 1.0 for both terminations, which corresponds to the charging effect by one excess Li-ion in our model. The mixed-COOH termination was about 0.8 lower than the corresponding case of H-termination. This is due to Li^+ bridging between the O atoms in the terminations and the CO_3^{2-} moieties in SEI, and the charge transfer from SEI to anode results in strong stability of interface. C atoms consisting of graphite were decreased during the intercalation process for any case, which were significant among edge region (z>-2.0). This

tendency was also seen in migrated Li shown in Fig. 8 though the variation range is different. In case of the H-termination, gross population of C atoms decreases upon the intercalation process and that of interfacial H increases, of which absolute variation are similar. Hydrogen termination on the other side showed less change. These results suggest that, associated with Li^+ intercalation from SEI to graphite, polarized electron at interfacial H moves into graphite. In case of the mixed-COOH termination, gross population of C atoms consisting of graphite decreases upon the intercalation process in similar to the case of H-termination, while that of interfacial H doesn't show large variation. Alternatively, that of C atoms in the functional group increases with intercalation. In other words, the functional group instead of interfacial H plays the electron donating role.

References

S1 M. Bagouin, D. Guerard and A. Herold, *"Action of Li Vapor on Graphite," Compt. Rend. C,* 1966*,* **262**(7), 557–559. *in French. (Equi Diagram, Crys Structure; Experimental)*

S2 BIOVIA Materials Studio, Dassault Systèmes BIOVIA, accelrys.com/materials-studio.

S3 Y. Idemoto, J. W. Richardson, N. Koura, S. Kohara and C.-K. Loong, *J. Phys. Chem. Solids,* 1998, **59,** 363-376.

S4 *NIST Chemistry WebBook, NIST Standard Reference Database Number 69,* ed. P. J. Linstrom and W. G. Mallar, National Institute of Standards and Technology, Gaithersburg MD, 20899.

S5 Y. Duan and D. C. Sorescu, *Phys. Rev. B,* 2009, **79,** 014301.

S6 S. Shi, Y. Qi, H. Li and L. G. Hector, *J. Phys. Chem. C,* 2013, **117,** 8579-8593.